ACS APPLIED MATERIALS & INTERFACES

Research Article

www.acsami.org

Facile Incorporation of Aggregation-Induced Emission Materials into Mesoporous Silica Nanoparticles for Intracellular Imaging and Cancer Therapy

Xiaoyong Zhang,[†,‡] Xiqi Zhang,[†,‡] Shiqi Wang,[‡] Meiying Liu,[§] Yun Zhang,[‡] Lei Tao,*[,‡] and Yen Wei*[,‡]

[‡]Department of Chemistry and the Tsinghua Center for Frontier Polymer Research, Tsinghua University, Beijing, 100084, P. R. China

[§]Beijing National Laboratory for Molecular Sciences (BNLMS), Key Laboratory of Organic Solids, Laboratory of New Materials, Institute of Chemistry, Chinese Academy of Sciences, Beijing 100190, China

Supporting Information

ABSTRACT: Aggregation-induced emission (AIE) materials were facilely incorporated into mesoporous silica nanoparticles (MSNs) via one-pot surfactant templated method. Cell imaging and cancer therapy applications of such fluorescent MSNs were further explored. We demonstrated that AIE-MSN nanocomposites showed strong fluorescence and uniform morphology, making them promising for both cell imaging and cancer therapy.

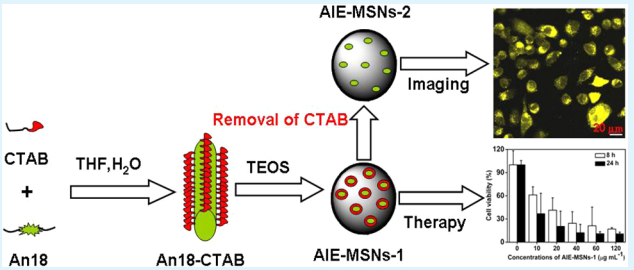

KEYWORDS: *aggregation-induced emission, mesoporous silica nanoparticles, cell imaging, cancer therapy, drug delivery, biomedical applications*

1. INTRODUCTION

The development of multifunctional nanoparticles (NPs) for biomedical applications has attracted many research interests over the past few decades.[1−3] Various materials with different functions have thus been integrated and widely used as multimodel bioprobes and targeted drug delivery systems.[4−8] Among them, the synthesis of multifunctional mesoporous silica nanoparticles (MSNs) has been intensively pursued due to their unique structural characteristics and superior properties including uniform and tunable pore structure, high surface area, simple surface functionalization, good dispersibility, excellent biocompatibility and cellular membrane-penetrating capacity.[9−18] It has been reported that numerous functional materials such as organic dyes, magnetic nanoparticles, or semiconductor quantum dots could be incorporated into MSNs, thus making them easily detactable in living organisms.[19−26] On the other hand, in chemotherapeutics area, polymers and targeting agents have also been introduced into MSNs to fabricate multifunctional MSNs.[27−38] Although the MSN-based nanosystems showed potential for various biomedical applications, their preparation procedures are rather complex and often require multisteps,[39−41] limiting the practical application of this promising material. Therefore, development of novel methods for facile preparation of multifunctional MSNs via straightforward procedure is still a challenge.

Different from conventional organic dyes, aggregation-induced emission (AIE) materials are an important and novel class of materials that emit more efficiently while in aggregated state than in dispersed state. Since Tang et al. reported on AIE materials in 2001, AIE-based materials have been widely investigated for various applications including organic light-emitting devices, chemosensors, biological imaging and so on.[42−51] In particular, the utilization of AIE-based materials for biological imaging applications have been extensively pursued in recent years.[52−55] Although AIE-based materials could overcome the issue of fluorescent quenching, their poor water solubility severely limited their practical biomedical applications. Modification of AIE materials with ions could improve their solubility in aqueous media, but the electric charges of the high concentrated ionized dyes may affect intracellular physiology and sometimes even kill the cells.A surface modified with nonionic surfactants could easily obtain water-soluble and biocompatible AIE bioprobes. However, it is still difficult to control the size and morphology of such AIE organic nanoparticles.[56] These organic nanoparticles are also normally physicochemically instable because of weak interactions between AIE dyes and surfactants.

In this contribution, we described the one-pot preparation of fluorescent MSNs using an AIE material **An18** (derivatived from 9,10-distyrylanthracene with alkoxyl end group) as fluorogens and a cationic surfactant cetyltrimethyl ammonium bromide (CTAB) as structure-directed template and cell killer agent. As shown in Scheme 1, **An18** and CTAB were first

Received: October 30, 2012
Accepted: January 30, 2013
Published: January 30, 2013

Scheme 1. Schematic showing the Preparation of AIE-MSNs and Their Utilized for Cell Imaging and Cancer Therapy Applications

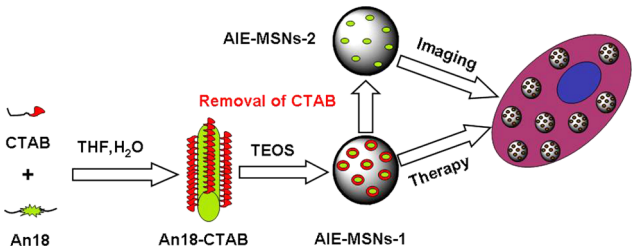

dispersed in tetrahydrofuran (THF) and H_2O. The amphiphilic complexes (**An18-CTAB**) could be easily formed with the increase of the water content in solution. The **An18-CTAB** could further serve as the structure direct template for preparation of MSNs. After removal of THF from the reaction systems, **An18-CTAB** was encapsulated in MSNs, thus making MSNs luminescent. To exploit the potential biomedical applications of **AIE-MSNs**, the cell imaging and cancer therapy applications of such **AIE-MSNs** were further investigated.

2. EXPERIMENTAL SECTION

2.1. Materials and Measurements. 9,10-Bis(chloromethyl)-anthracene purchased from TCI and 4-hydroxybenzaldehyde, 1-bromooctadecane, cetyltrimethylammonium bromide (CTAB), and tetraethylorthosilicate (TEOS) purchased from Alfa Aesar were used as received. All other agents and solvents were purchased from commercial sources and used directly without further purification. Tetrahydrofuran (THF) was distilled from sodium/benzophenone. Ultrapure water was used in the experiments. Intermediates **1**[57] and **2**[58] were prepared according to the literature methods. ^{1}H NMR and ^{13}C NMR spectra were measured on a JEOL 400 MHz spectrometer [$CDCl_3$ as solvent and tetramethylsilane (TMS) as the internal standard]. Standard FAB-MS was obtained on ZAB-HS mass spectrometry. Fluorescence spectra were measured on a PE LS-55 spectrometer with a slit width of 3 nm for both excitation and emission. Transmission electron microscopy (TEM) images were recorded on a JEM-1200EX microscope operated at 100 kV, the TEM specimens were made by placing a drop of the nanoparticles suspension on a carbon-coated copper grid. The FT-IR spectra were obtained in a transmission mode on a Perkin-Elmer Spectrum 100 spectrometer (Waltham, MA, USA). Typically, 4 scans at a resolution of 1 cm^{-1} were accumulated to obtain one spectrum. Powder X-ray diffraction (XRD) measurements were made on Bruker D8 Advance X-ray power diffractometer using Cu Kα radiation (λ = 1.5406 Å). Brunauer–Emmett–Teller (BET) surface area, S_{BET}, of the samples was determined from N_2 adsorption–desorption isotherms obtained at 77 K using an ASAP 2010 Suface Area Analyzer (Micromeritics Instrument, USA). Prior to measurement, all samples were outgassed for 2 h at 473 K and 0.1 Pa. Surface areas were calculated by the BET method.

2.2. Preparation of AIE-MSNs. CTAB (0.50 g, 1.37 mmol) was dissolved in 250 mL of ultrapure water. Sodium hydroxide aqueous solution (2.00 M, 1.80 mL) and **An18** (0.10 g, 0.11 mmol) in THF were introduced to the CTAB solution. The temperature of the mixture was adjusted to 80 °C. Then tetraethoxysilane (TEOS, 5.00 mL, 22.4 mmol) was added dropwise to the surfactant solution under vigorous stirring. The mixture was allowed to react for 4 h to give rise to a white precipitate. This solid crude product was filtered, washed with deionized water and methanol for several times and dried in vacuum drying oven at 35 °C to yield **AIE-MSNs-1**. To remove the surfactant CTAB, we refluxed 1.00 g of the assynthesized **AIE-MSNs-1** for 24 h in a methanolic solution of 6.00 mL of HCl (37.4%) in 100.00 mL of methanol. The resulting material was filtered and extensively washed with deionized water and methanol several times and dried in vacuum drying oven at 35 °C to yield **AIE-MSNs-2**.

Scheme 2. Chemical Structure of An18

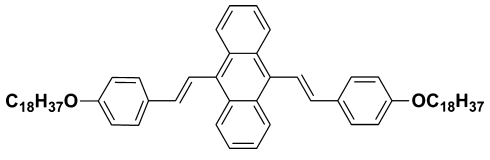

2.3. Cytotoxicity of AIE-MSNs NPs. Cell morphology was observed to examine the effects of **AIE-MSNs** NPs to A549 cells. Briefly, cells were seeded in 6-well microplates at a density of 1 × 10^5 cells mL^{-1} in 2 mL of respective media containing 10% fetal bovine serum (FBS). After cell attachment, plates were washed with PBS and the cells were treated with complete cell culture medium, or different concentrations of fluoridated **AIE-MSNs** NPs prepared in 10% FBS containing media for 8 and 24 h. Then all samples were washed with PBS three times to remove the uninternalized NPs. The morphology of cells was observed by using an optical microscopy (Leica, Germany), the overall magnification was ×100.

The cell viability of **AIE-MSNs** NPs on A549 cells was evaluated by cell counting kit-8 (CCK-8) assay based on our previous reports.[59] Briefly, cells were seeded in 96-well microplates at a density of 5 × 10^4 cells mL^{-1} in 160 μL of respective media containing 10% FBS. After 24 h of cell attachment, the cells were incubated with 10, 20, 40, 60, 100 μg mL^{-1} **AIE-MSNs-1** or 10, 20, 40, 80, 120 μg mL^{-1} **AIE-MSNs-2** NPs for 8 and 24 h. Then nanoparticles were removed and cells were washed with PBS three times. Ten microliters of CCK-8 dye and 100 μL of DMEM cell culture medium were added to each well and incubated for 2 h at 37 °C. Plates were then analyzed with a microplate reader (VictorIII, Perkin-Elmer). Measurements of formazan dye absorbance were carried out at 450 nm, with the reference wavelength at 620 nm. The values were proportional to the number of live cells. The percent reduction of CCK-8 dye was compared to controls (cells not exposure to **AIE-MSN** NPs), which represented 100% CCK-8 reduction. Three replicate wells were used per microplate, and the experiment was repeated three times. Cell survival was expressed as absorbance relative to that of untreated controls. Results are presented as mean ± standard deviation (SD).

2.4. Confocal Microscopic Imaging of Cells Using AIE-MSNs. A549 cells were cultured in Dulbecco's modified eagle medium (DMEM) supplemented with 10% heat-inactivated FBS, 2 mM glutamine, 100 U mL^{-1} penicillin, and 100 μg mL^{-1} of streptomycin. Cell culture was maintained at 37 °C in a humidified condition of 95% air and 5% CO_2 in culture medium. Culture medium was changed every three days for maintaining the exponential growth of the cells. On the day prior to treatment, cells were seeded in a glass bottom dish with a density of 1 × 10^5 cells per dish. On the day of treatment, the cells were incubated with **AIE-MSNs-2** NPs at a final concentration of 50 μg mL^{-1} for 3 h at 37 °C. Afterward, the cells were washed three times with PBS to remove the **AIE-MSNs-2** NPs and then fixed with 4% paraformaldehyde for 10 min at room temperature. Cell images were taken with a confocal laser scanning microscope (CLSM) Zesis 710 3-channel (Zesis, Germany) with the excitation wavelengths of 405 nm.

3. RESULTS AND DISCUSSIONS

3.1. Charcterization of AIE-MSNs. The AIE fluorogen **An18** was prepared following the synthetic route shown in Scheme S1 in the Supportng Information. Its structure was characterized and confirmed by standard spectroscopic methods. As shown in our previous report, by mixing of **An18** and Pluronic F127, water-soluble and biocompatible fluorescent organic nanoparticles (**An18-F127**) could be facilely obtained.[56] The **An18-F127** NPs emitted strong fluorescence in water with the FL intensity obviously stronger than that in a pure THF solution. In this report, significant

dx.doi.org/10.1021/am302512u | ACS Appl. Mater. Interfaces 2013, 5, 1943–1947

fluorescent enhancement was also found when **An18** was surface modified using a cationic surfactant CTAB. And **An18-CTAB** could be further incorporated into MSNs to form a novel fluorescent NPs (**AIE-MSNs**). Compared with previous reports, the morphology of the **AIE-MSNs** is more controllable and stable.[56] As shown in Figure 1a, **AIE-MSNs** have a

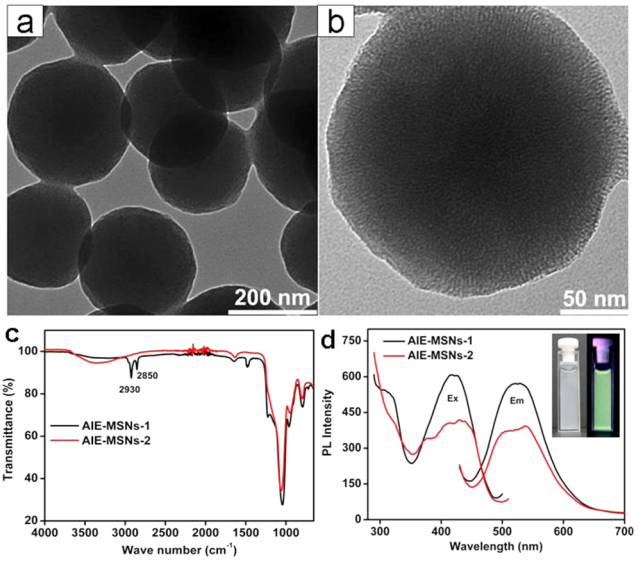

Figure 1. Characterization of **AIE-MSNs**. (a, b) TEM images of AIE-MSNs-1. (c) FT-IR spectra of **AIE-MSNs-1** and **AIE-MSNs-2**, (d) excitation and emission (excited by wavelength of 405 nm) spectra of **AIE-MSNs-1** and **AIE-MSNs-2**, the insets are images of **AIE-MSNs-2** dispersed in water (left) and excited by UV lamp (λ = 365 nm, right).

spherical shape and uniform particle size (about 200 nm). High-resolution transmission electron microscopy (TEM) images further demosntrated that MSNs exhibited highly ordered mesoporous channels (Figure 1b). It is worth noting that the morphology and structural characteristics of **An18-CTAB**-templated MSNs showed no significant difference with those of CTAB templated MSNs (see Figure S1 in the Supporting Information). Figure 1c shows the Fourier transform infrared (FT-IR) spectra of **AIE-MSNs** before (**AIE-MSNs-1**) and after (**AIE-MSNs-2**) removal of surfactants CTAB (washing with methanol and diluted hydrochloric acid). The characteristic peaks located at 1060, 962, and 793 cm^{-1} corresponding to the Si−O band were observed in both of **AIE-MSNs**. However, as compared with **AIE-MSNs-1**, the stretching vibration bands of C−H which located at 2930 and 2850 cm^{-1} were disappeared in the sample of **AIE-MSNs-2**, evidencing the successful removal of CTAB. The N2 adsorption−desorption isotherms were determined at various relative pressures (P/P_0) on **AIE-MSNs-1** and **AIE-MSNs-2** (see Figure S3 in the Supporting Information). The BET surface areas of **AIE-MSNs-1** and **AIE-MSNs-2** are 243.2 and 657.7 m^2/g, respectively. The pore diameter of **AIE-MSNs** was increased from 3.12 to 5.03 nm after removal of surfactant (CTAB), which is well consistent with the proe diameter of MCM41 without encapsulation of **An18**.The BET results demonstrated that **AIE-MSNs** still possessed large surface areas after removal of CTAB, which is very useful for loading other image or therapy agents. More important, we also found that **AIE-MSNs-2** is still fluorescent. As shown in the insets of Figure 1d, green-yellow fluorescence could be clearly observed when **AIE-MSNs-2** water dispersion was excited by UV lamp (λ = 365 nm). Furthermore, the excitation and emission spectra of **AIE-MSNs-1** and **AIE-MSNs-2** were displayed in Figure 1d. Compared with the PL spectra of **AIE-MSNs-1**, the fluorescent intensity of **AIE-MSNs-2** has decreased in some extent, which is likely ascribed to the leaching of **An18** in the process of surfactant removal. On the other hand, the emission spectra of **AIE-MSNs-2** was divided into two peaks, and the intensity at long wavelenght was relatively enhenced, which reflected the different aggragate state of **An18** before and after removal of surfactant. This phenomenon was also observed in our recent report.[60] Finally, The original of emission and excitation bands is possible ascribed to the restricted intramolecular rotation of **An18** as proposed by Tang et al.[43] Taken together, all of these results suggested that **An18** dye was still encapsulated in MSNs after removal of CTAB. As compared with the AIE based organic NPs, **AIE-MSNs-2** showed uniform morphology and high surface areas, which should be more promising for biological imaging and drug delivery applications.

3.2. Biocompatibility of AIE-MSNs-2. To exploit its potential biomedical applications, the biocompatibility of **AIE-MSNs-2** was determined.[59,61] Figure 2a−c show the optical

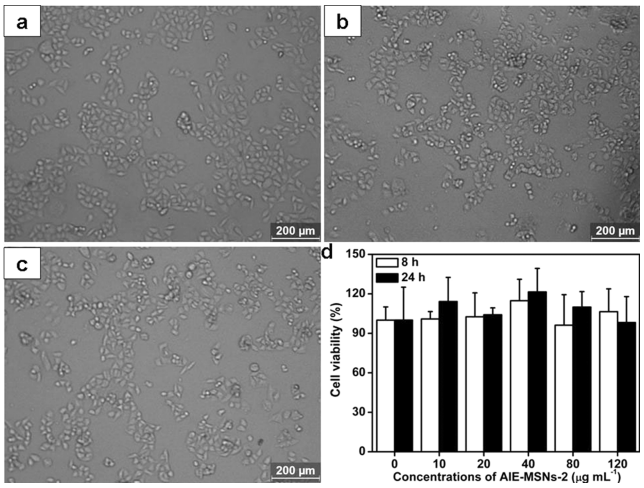

Figure 2. Biocompatibility evaluation of **AIE-MSNs-2**. (a−c) Optical microscopy images of A549 cells incubated with different concentrations of **AIE-MSNs-2** for 24 h: (a) control cells, (b) 40 $\mu g\ mL^{-1}$, (c) 120 $\mu g\ mL^{-1}$; (d) time- and dose-dependent cell viability of AIE-MSNs-2 with A549 cells.

microscopy images of A549 cells after their incubation with **AIE-MSNs-2** for 24 h. Compared with the control group (cells without **AIE-MSNs-2**), all cells still kept their normal morphology even the concentration of **AIE-MSNs-2** is as high as 120 $\mu g\ mL^{-1}$. These observations gave us preliminary impression that **AIE-MSNs-2** is biocompatibile with cells. Cell viability results from WST assay further demonstrated the excellent biocompatibility of **AIE-MSNs-2**. As shown in Figure 2d, no obvious cell viability decrease was observed via cell viability examination. Even the concentration of **AIE-MSNs-2** reached up to 120 $\mu g\ mL^{-1}$, the cell viability was still greater than 95%. All the above results confirmed the excellent biocompatibility and potential biological imaging applications of **AIE-MSNs-2**.

3.3. Cell Imaging of AIE-MSNs-2. Figure 3 shows the CLSM images of cells after incubating them with 50 $\mu g\ mL^{-1}$ of **AIE-MSNs-2** for 3 h.[62,63] The cell internalized **AIE-MSNs-2**

dx.doi.org/10.1021/am302512u | ACS Appl. Mater. Interfaces 2013, 5, 1943−1947

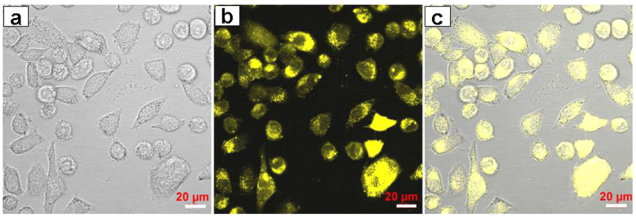

Figure 3. CLSM images of A549 cells incubated with 50 μg mL^{-1} of **AIE-MSNs-2** for 3 h. (a) Bright field, (b) excited with 405 nm laser, (c) merge image of a and b.

can be excited by laser with 405 nm excitation, and emitted green-yellow fluorescence. The fluorescent areas were overlapped on the locations of cells (Figure 3a), indicating that **AIE-MSNs-2** could be uptaken by cells and accumulated in cells. From CLSM images, many dark areas were also found within the cells, which may be the locations of cell nucleus. Based on CLSM images, conclusion could be drawn that **AIE-MSNs-2** could translocate into cells and locate at cytoplasm. Given its excellent biocompatibility and strong fluorescence, such novel fluorescent nanomaterials should be a promising and alternative bioprobe for bioimaging applications.

3.4. Cancer Therapy of AIE-MSN-1. On the other hand, CTAB has been regarded as a broad-spectrum antiseptic agent and cheap tumoricidal agent. Emma ito et al. have recently identified pure CTAB as a potential cancer-specific compound against head and neck cancer cell lines with the minimal cytotoxicity against normal fibroblasts.[64] Its possible anticancer mechanism is ascribed to the cell apoptosis promoting effect of CTAB. More recently, the incorporation of CTAB into mesoporous silica nanoparticles has also been reported by Shi et al.[65] In the current work, the anticancer effectiveness of **AIE-MSNs-1** to A549 cells was also determined. As shown in Figure 4, a lot of cells turned round after incubation with 10 μg mL^{-1} of **AIE-MSNs-1** for 8 h. When the concentrations of **AIE-MSNs-1** increased to 60 μg mL^{-1}, almost no cells were found by optical microscopy observation. These results preliminary evidenced the significant cytotoxicity of **AIE-MSNs-1**. The anticancer effectiveness was further quantitatively determined by WST assay. Well consistent with optical microscopy observation, significant cell viability decrease was found when cells incubated with only 10 μg mL^{-1} of **AIE-MSNs-1** for 8 h. On the basis of WST results, the half maximal effective concentration (EC50) values of **AIE-MSNs-1** to A549 cells were 14.4 and 3.5 μg mL^{-1} for 8 and 24 h incubation, respectively. Furthermore, the cytotoxicity of free CTAB to A549 was also determined. As displayed in Figure S4 in the Supporting Information, free CTAB shows more significant cytotoxicity to A549 cells. The EC50 of CTAB to A549 were 4.41 and 1.83 μg mL^{-1} for 8 and 24 h incubation, respectively. In an independent experiment, the mass percent of CTAB loaded on the **AIE-MSNs** was also calculated to be 34%, which is well consistent with the EC50 ratios of CTAB to **AIE-MSNs-1**. These results implied that the CTAB was the main anticancer component of **AIE-MSNs-1**. Combined with the features of **An18**, CTAB and MSNs, **AIE-MSNs-1** with remarkable anticancer effectiveness should be a multifunctional nanohybrids promising for cancer therapy.

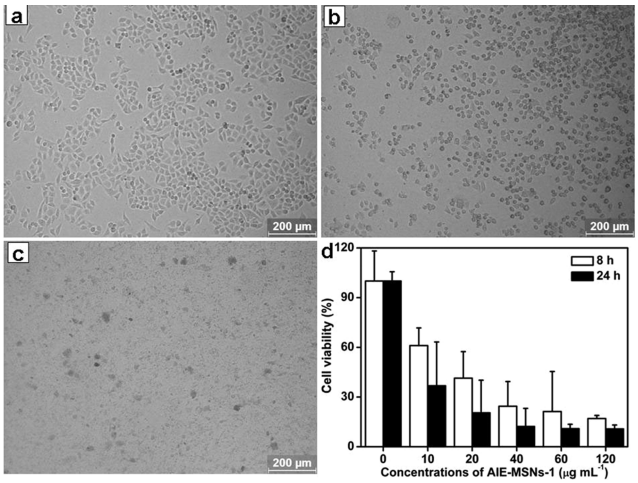

Figure 4. (a–c) Optical microscopy of A549 cells incubated with different concentrations of **AIE-MSNs-1** for 8 h: (a) control cells, (b) 10 μg mL^{-1}, (c) 60 μg mL^{-1}, (d) cell viability of **AIE-MSNs-1**. A549 cells were incubated with different concentrations of **AIE-MSNs-1** for 8 and 24 h. The values of EC50 are 14.4 and 3.5 μg mL^{-1} for 8 and 24 h incubation, respectively.

4. CONCLUSIONS

In summary, AIE-MSNs were prepared via one-pot encapsulation of AIE dye (An18) into MSNs using CTAB as both surfactant template and cell killer agent. **AIE-MSNs-1** (without removal of surfactant) exhibited remarkable anticancer effectiveness with EC50 value of 3.5 μg mL^{-1} for 24 h, indicating their potential cancer therapy applications. On the other hand, after removal of CTAB (**AIE-MSNs-2**), **An18** was still encapsulated in MSNs thus leading to formation of uniform luminescent silica nanoparticles. Such novel fluorescent MSNs showed excellent biocompatibility with A549 cells and can be utilized for cell imaging applications. Thus, given the facile preparation procedure and combination properties of **An18**, CTAB, and MSNs, **AIE-MSNs** are expected to be promising for cell imaging, cancer therapy, and other biomedical applications.

■ ASSOCIATED CONTENT

Supporting Information

^{1}H NMR of An18 and TEM images of MSNs. This material is available free of charge via the Internet at http://pubs.acs.org.

■ AUTHOR INFORMATION

Corresponding Author

*E-mail: leitao@mail.tsinghua.edu.cn; weiyen@tsinghua.edu.cn.

Author Contributions

†These authors contributed equally to this work.

Notes

The authors declare no competing financial interest.

■ ACKNOWLEDGMENTS

This research was supported by the National Science Foundation of China (no.21134004, 21104039, 21201108), and the National 973 Project (2011CB935700), China Postdoctoral Science Foundation (2011M500280, 2012 M520243).

■ REFERENCES

(1) Farokhzad, O. C.; Langer, R. *Adv. Drug Delivery Rev.* **2006**, *58*, 1456–1459.

(2) Riehemann, K.; Schneider, S. W.; Luger, T. A.; Godin, B.; Ferrari, M.; Fuchs, H. *Angew. Chem., Int. Ed.* **2009**, *48*, 872–897.

(3) Mout, R.; Moyano, D. F.; Rana, S.; Rotello, V. M. *Chem. Soc. Rev.* **2012**, *41*, 2539−2544.
(4) Boisselier, E.; Astruc, D. *Chem. Soc. Rev.* **2009**, *38*, 1759−1782.
(5) Calderón, M.; Dagia, N. M.; Haag, R. *Chem. Soc. Rev.* **2012**, *41*, 2824−2848.
(6) Sena, M.; Gao, X. *Chem. Soc. Rev.* **2010**, *39*, 4326−4354.
(7) Gupta, A. K.; Gupta, M. *Biomaterials* **2005**, *26*, 3995−4021.
(8) Hui, J.; Zhang, X.; Zhang, Z.; Wang, S.; Tao, L.; Wei, Y.; Wang, X. *Nanoscale* **2012**, *4*, 6967−6970.
(9) Patel, K.; Angelos, S.; Dichtel, W. R.; Coskun, A.; Yang, Y. W.; Zink, J. I.; Stoddart, J. F. *J. Am. Chem. Soc.* **2008**, *130*, 2382−2383.
(10) He, X.; Hai, L.; Su, J.; Wang, K.; Wu, X. *Nanoscale* **2011**, *3*, 2936−2942.
(11) Li, Z.; Barnes, J. C.; Bosoy, A.; Stoddart, J. F.; Zink, J. I. *Chem. Soc. Rev.* **2012**, *41*, 2590−2605.
(12) Popat, A.; Hartono, S. B.; Stahr, F.; Liu, J.; Qiao, S. Z.; Lu, G. Q. M. *Nanoscale* **2011**, *3*, 2801−2818.
(13) Ambrogio, M. W.; Thomas, C. R.; Zhao, Y. L.; Zink, J. I.; Stoddart, J. F. *Acc. Chem. Res.* **2010**, *44*, 903−913.
(14) Rosenholm, J. M.; Sahlgren, C.; Lindén, M. *Nanoscale* **2010**, *2*, 1870−1883.
(15) Thomas, C. R.; Ferris, D. P.; Lee, J. H.; Choi, E.; Cho, M. H.; Kim, E. S.; Stoddart, J. F.; Shin, J. S.; Cheon, J.; Zink, J. I. *J. Am. Chem. Soc.* **2010**, *132*, 10623−10625.
(16) Nguyen, T. D.; Liu, Y.; Saha, S.; Leung, K. C. F.; Stoddart, J. F.; Zink, J. I. *J. Am. Chem. Soc.* **2007**, *129*, 626−634.
(17) Zhao, D.; Feng, J.; Huo, Q.; Melosh, N.; Fredrickson, G. H.; Chmelka, B. F.; Stucky, G. D. *Science* **1998**, *279*, 548−552.
(18) Zhao, D.; Huo, Q.; Feng, J.; Chmelka, B. F.; Stucky, G. D. *J. Am. Chem. Soc.* **1998**, *120*, 6024−6036.
(19) Johnson, N. J. J.; Sangeetha, N. M.; Boyer, J. C.; van Veggel, F. C. J. M. *Nanoscale* **2010**, *2*, 771−777.
(20) Shan, Y.; Xu, J. J.; Chen, H. Y. *Nanoscale* **2011**, *3*, 2916−2923.
(21) Hui, C.; Shen, C.; Tian, J.; Bao, L.; Ding, H.; Li, C.; Tian, Y.; Shi, X.; Gao, H. J. *Nanoscale* **2011**, *3*, 701−705.
(22) Zhang, F.; Braun, G. B.; Shi, Y.; Zhang, Y.; Sun, X.; Reich, N. O.; Zhao, D.; Stucky, G. *J. Am. Chem. Soc.* **2010**, *132*, 2850−2851.
(23) Yang, J.; Deng, Y.; Wu, Q.; Zhou, J.; Bao, H.; Li, Q.; Zhang, F.; Li, F.; Tu, B.; Zhao, D. *Langmuir* **2010**, *26*, 8850−8856.
(24) Zhou, L.; Yuan, J.; Wei, Y. *J. Mater. Chem.* **2010**, *21*, 2823−2840.
(25) Gan, Q.; Lu, X.; Yuan, Y.; Qian, J.; Zhou, H.; Shi, J.; Liu, C. *Biomaterials* **2011**, *32*, 1932−1942.
(26) Wu, H.; Liu, G.; Zhang, S.; Shi, J.; Zhang, L.; Chen, Y.; Chen, F.; Chen, H. *J. Mater. Chem.* **2011**, *21*, 3037−3045.
(27) Couleaud, P.; Morosini, V.; Frochot, C.; Richeter, S.; Raehm, L.; Durand, J. O. *Nanoscale* **2010**, *2*, 1083−1095.
(28) He, Q.; Shi, J.; Chen, F.; Zhu, M.; Zhang, L. *Biomaterials* **2009**, *31*, 3335−3346.
(29) Cotí, K. K.; Belowich, M. E.; Liong, M.; Ambrogio, M. W.; Lau, Y. A.; Khatib, H. A.; Zink, J. I.; Khashab, N. M.; Stoddart, J. F. *Nanoscale* **2009**, *1*, 16−39.
(30) Morelli, C.; Maris, P.; Sisci, D.; Perrotta, E.; Brunelli, E.; Perrotta, I.; Panno, M. L.; Tagarelli, A.; Versace, C.; Casula, M. F. *Nanoscale* **2011**, *3*, 3198−3207.
(31) Brühwiler, D. *Nanoscale* **2010**, *2*, 887−892.
(32) Xu, M.; Feng, D.; Dai, R.; Wu, H.; Zhao, D.; Zheng, G. *Nanoscale* **2011**, *3*, 3329−3333.
(33) Bao, H.; Yang, J.; Huang, Y.; Xu, Z. P.; Hao, N.; Wu, Z.; Lu, G. Q. M.; Zhao, D. *Nanoscale* **2011**, *3*, 4069−4073.
(34) He, Q.; Gao, Y.; Zhang, L.; Zhang, Z.; Gao, F.; Ji, X.; Li, Y.; Shi, J. *Biomaterials* **2011**, *32*, 7711−7720.
(35) Chen, Y.; Chen, H.; Ma, M.; Chen, F.; Guo, L.; Zhang, L.; Shi, J. *J. Mater. Chem.* **2011**, *21*, 5290−5298.
(36) Chen, C.; Geng, J.; Pu, F.; Yang, X.; Ren, J.; Qu, X. *Angew. Chem., Int. Ed.* **2011**, *50*, 882−886.
(37) Chen, C.; Pu, F.; Huang, Z.; Liu, Z.; Ren, J.; Qu, X. *Nucleic Acids Res.* **2011**, *39*, 1638−1644.
(38) Yang, X.; Liu, X.; Liu, Z.; Pu, F.; Ren, J.; Qu, X. *Adv. Mater.* **2012**, *24*, 2890−2895.
(39) Zhao, W.; Gu, J.; Zhang, L.; Chen, H.; Shi, J. *J. Am. Chem. Soc.* **2005**, *127*, 8916−8917.
(40) Xing, H.; Bu, W.; Zhang, S.; Zheng, X.; Li, M.; Chen, F.; He, Q.; Zhou, L.; Peng, W.; Hua, Y. *Biomaterials* **2011**, *33*, 1079−1089.
(41) Mahtab, F.; Lam, J. W. Y.; Yu, Y.; Liu, J.; Yuan, W.; Lu, P.; Tang, B. Z. *Small* **2011**, *7*, 1448−1455.
(42) Zhang, X.; Chi, Z.; Li, H.; Xu, B.; Li, X.; Zhou, W.; Liu, S.; Zhang, Y.; Xu, J. *Chem.-Asian J.* **2011**, *6*, 808−811.
(43) Luo, J.; Xie, Z.; Lam, J. W. Y.; Cheng, L.; Chen, H.; Qiu, C.; Kwok, H. S.; Zhan, X.; Liu, Y.; Zhu, D.; Tang, B. Z. *Chem. Commun.* **2001**, *37*, 1740−1741.
(44) Yang, Z.; Chi, Z.; Yu, T.; Zhang, X.; Chen, M.; Xu, B.; Liu, S.; Zhang, Y.; Xu, J. *J. Mater. Chem.* **2009**, *19*, 5541−5546.
(45) Chi, Z.; Zhang, X.; Xu, B.; Zhou, X.; Ma, C.; Zhang, Y.; Liu, S.; Xu, J. *Chem. Soc. Rev.* **2012**, *48*, 3878−3896.
(46) Zhao, Z.; Chen, S.; Shen, X.; Mahtab, F.; Yu, Y.; Lu, P.; Lam, J. W. Y.; Kwok, H. S.; Tang, B. Z. *Chem. Commun.* **2010**, *46*, 686−688.
(47) Hong, Y.; Lam, J. W. Y.; Tang, B. Z. *Chem. Soc. Rev.* **2011**, *40*, 5361−5388.
(48) Zhang, X.; Yang, Z.; Chi, Z.; Chen, M.; Xu, B.; Wang, C.; Liu, S.; Zhang, Y.; Xu, J. *J. Mater. Chem.* **2009**, *20*, 292−298.
(49) An, B. K.; Lee, D. S.; Lee, J. S.; Park, Y. S.; Song, H. S.; Park, S. Y. *J. Am. Chem. Soc.* **2004**, *126*, 10232−10233.
(50) Zhang, X.; Chi, Z.; Li, H.; Xu, B.; Li, X.; Liu, S.; Zhang, Y.; Xu, J. *J. Mater. Chem.* **2011**, *21*, 1788−1796.
(51) Zhang, X.; Chi, Z.; Xu, B.; Chen, C.; Zhou, X.; Zhang, Y.; Liu, S.; Xu, J. *J. Mater. Chem.* **2012**, *22*, 18505−18513.
(52) Qin, W.; Ding, D.; Liu, J.; Yuan, W. Z.; Hu, Y.; Liu, B.; Tang, B. Z. *Adv. Funct. Mater.* **2012**, *22*, 771−779.
(53) Zhao, Z.; Geng, J.; Chang, Z.; Chen, S.; Deng, C.; Jiang, T.; Qin, W.; Lam, J. W. Y.; Kwok, H. S.; Qiu, H. *J. Mater. Chem.* **2012**, *22*, 11018−11021.
(54) Mahtab, F.; Yu, Y.; Lam, J. W. Y.; Liu, J.; Zhang, B.; Lu, P.; Zhang, X.; Tang, B. Z. *Adv. Funct. Mater.* **2012**, *21*, 1733−1740.
(55) Geng, J.; Li, K.; Ding, D.; Zhang, X.; Qin, W.; Liu, J.; Tang, B. Z.; Liu, B. *Small* **2012**, *8*, 3655−3663.
(56) Zhang, X.; Zhang, X.; Wang, S.; Liu, M.; Tao, L.; Wei, Y. *Nanoscale* **2013**, *5*, 147−150.
(57) Wang, C.; Wang, G.; Wang, Z.; Zhang, X. *Chem.—Eur. J.* **2011**, *17*, 3322−3325.
(58) Zhang, H. C.; Guo, E. Q.; Zhang, Y. L.; Ren, P. H.; Yang, W. J. *Chem. Mater.* **2009**, *21*, 5125−5135.
(59) Zhang, X.; Qi, H.; Wang, S.; Feng, L.; Ji, Y.; Tao, L.; Li, S.; Wei, Y. *Toxicol. Res.* **2012**, *1*, 201−205.
(60) Zhang, X.; Chi, Z.; Xu, B.; Jiang, L.; Zhou, X.; Zhang, Y.; Liu, S.; Xu, J. *Chem. Commun.* **2012**, *48*, 10895−10897.
(61) Zhang, X.; Hu, W.; Li, J.; Tao, L.; Wei, Y. *Toxicol. Res.* **2012**, *1*, 62−68.
(62) Zhang, X.; Wang, S.; Xu, L.; Ji, Y.; Feng, L.; Tao, L.; Li, S.; Wei, Y. *Nanoscale* **2012**, *4*, 5581−5584.
(63) Zhang, X.; Wang, S.; Fu, C.; Feng, L.; Ji, Y.; Tao, L.; Li, S.; Wei, Y. *Polymer Chem.* **2012**, *3*, 2716−2719.
(64) Ito, E.; Yip, K. W.; Katz, D.; Fonseca, S. B.; Hedley, D. W.; Chow, S.; Xu, G. W.; Wood, T. E.; Bastianutto, C.; Schimmer, A. D. *Mol. Pharm.* **2009**, *76*, 969−983.
(65) He, Q.; Shi, J.; Chen, F.; Zhu, M.; Zhang, L. *Biomaterials* **2010**, *31*, 3335−3346.